



**HAL**  
open science

## The structure of chromophore-grafted Amyloid- $\beta$ 12-28 dimers in the gas-phase: FRET-experiments guided modelling

Alexander Kulesza, Steven Daly, Chang Min Choi, Anne-Laure Simon, Fabien Chirot, Luke Macaleese, Rodolphe Antoine, Philippe Dugourd

► **To cite this version:**

Alexander Kulesza, Steven Daly, Chang Min Choi, Anne-Laure Simon, Fabien Chirot, et al.. The structure of chromophore-grafted Amyloid- $\beta$  12-28 dimers in the gas-phase: FRET-experiments guided modelling. *Physical Chemistry Chemical Physics*, 2016, 18 (13), pp.9061-9069. 10.1039/c6cp00263c . hal-01344513

**HAL Id: hal-01344513**

**<https://hal.science/hal-01344513>**

Submitted on 12 Jul 2016

**HAL** is a multi-disciplinary open access archive for the deposit and dissemination of scientific research documents, whether they are published or not. The documents may come from teaching and research institutions in France or abroad, or from public or private research centers.

L'archive ouverte pluridisciplinaire **HAL**, est destinée au dépôt et à la diffusion de documents scientifiques de niveau recherche, publiés ou non, émanant des établissements d'enseignement et de recherche français ou étrangers, des laboratoires publics ou privés.



## The structure of chromophore-grafted Amyloid- $\beta_{12-28}$ dimers the gas-phase: FRET-experiments guided modelling

Alexander Kulesza<sup>a,b</sup>, Steven Daly<sup>a,b</sup>, Chang Min Choi<sup>a,b</sup>, Anne-Laure Simon<sup>a,b</sup>, Fabien Chirot<sup>a,c</sup>, Luke MacAleese<sup>a,b</sup>, Rodolphe Antoine<sup>a,b</sup>, Philippe Dugourd<sup>a,b,†</sup>

Received 00th January 20xx,  
Accepted 00th January 20xx

DOI: 10.1039/C6CP00263C

[www.rsc.org/](http://www.rsc.org/)

We present theoretical modelling, ion mobility spectrometry and action-FRET experiments for chromophore-grafted Amyloid- $\beta_{12-28}$  dimers. A first-principles global minimum search based on replica-exchange molecular dynamics (REMD) leads to a compact structure with strong interstrand interaction. We use REMD with a distance restraint that implements an adaptive effective bias upon average FRET-efficiencies and thus guides the sampling by the action-FRET measurement. This procedure leads to a pair of weakly interacting peptides. Ion-mobility confirms that the weakly interacting structure and not the global minimum with strongly interacting peptides is populated in the experiment. The presence of a high energy barrier between the two structural families, as evidenced from the MD data, suggests that a kinetically trapped structure is observed in the experiment.

### Introduction

A commonality among severe neuropathological conditions like Alzheimer's, Parkinson's, Huntington's and prion diseases appears to be that cause and symptoms are directly linked on a molecular level – soluble oligomers responsible for synaptic dysfunction aggregate and build up large, insoluble deposits.<sup>1</sup> The role of the Amyloid- $\beta$  (A $\beta$ ) peptide for Alzheimer's disease (AD), taken as prominent example, has been subject of active research<sup>2</sup>. Investigations on the interplay between oligomers, fibrils and AD<sup>3-8</sup> let researchers recognize that A $\beta$  aggregation itself is a pharmacological target<sup>9</sup>, but until now no cure is available to treat this condition effectively. A detailed understanding of the interactions, the aggregation process and influential factors on the molecular level will accelerate the development of cures for conditions caused by protein misfolding and aggregation.

Since the gas-phase is a well-defined environment that allows to access intrinsic properties of selected species without solvent interactions or external effects, structural investigations in this medium seem highly attractive to obtain insight into the aggregation characteristics. Over the last decades, the coupling of ion mobility spectrometry (IMS) and mass spectrometry has been one of the powerful analytical techniques used to separate and identify biomolecules on the basis of structural differences.<sup>10,11</sup> IMS has been used to

understand the overall structure and folding process of native proteins – often accompanied by theoretical studies<sup>10-20</sup>. Successful applications of IMS to structurally characterize intrinsically disordered proteins<sup>21,22</sup> (especially in frame of Amyloid formation<sup>19,20,23</sup>) and the ability to tune experimental parameters so as to preserve native conformational populations<sup>24</sup>, suggest to use IMS as an accurate measure of A $\beta$  aggregation. In particular, issues arising from crosslinking during gel-electrophoresis separations of A $\beta$  can be resolved using IMS<sup>25,26</sup>. Thus, although several mechanistic questions (e.g. the effect of solvation<sup>27</sup>) cannot be addressed by this technique, the complementarity of the gas-phase approach is valuable for linking and validating solution versus gas-phase populations.

Additionally, an optical technique widely used in structural biology – Förster Resonant Energy Transfer (FRET)<sup>28-30</sup> – has been transposed to the gas-phase<sup>31-35</sup>. Action-FRET<sup>32</sup> reveals the efficiency of electronic excitation energy being transferred from a donor chromophore to an acceptor moiety by its fragmentation. According to Förster Theory, this efficiency depends on the distance of donor and acceptor to the reciprocal sixth power, and it is regarded as a tool for distance measurement (and sometimes termed the molecular ruler<sup>36,37</sup>).

Structural modelling is an integral part of these two structure-sensitive experiments: predictions based on structural models of the molecules enable interpretation and assignment of biomolecular conformations to the experiments.

Modelling can start from atomically resolved experiment-derived structural representations (e.g. structures modelled by exploiting NMR spectroscopy-derived restraints<sup>38,39</sup>; for a recent overview on experiments-restrained modelling of RNA structure see ref.<sup>40</sup>). Also FRET-restrained structural modelling

<sup>a</sup> Université de Lyon, F-69622, Lyon, France.

<sup>b</sup> CNRS et Université Lyon 1, UMR5306, Institut Lumière Matière.

<sup>c</sup> CNRS et Université Lyon 1 UMR 5280, Institut des Sciences Analytiques

† E-mail: philippe.dugourd@univ-lyon1.fr

Electronic Supplementary Information (ESI) available: Monomer starting configurations, convergence and trajectory mobility in REMD sampling, simulations in solvent. See DOI: 10.1039/c6cp00263c

has become popular thanks to the work of Seidel and coworkers<sup>41</sup>.

Among theoretical work concerning the aggregation of the A $\beta$  peptide, notably, all-atom MD simulations investigated implications of A $\beta$ 's folding landscape onto aggregation<sup>42</sup> and the stability of A $\beta$ <sub>18-22</sub> aggregates up to the 32 mer<sup>43</sup>. Likewise, the dimerization of the full-length A $\beta$  has been elucidated<sup>44</sup> and the  $\alpha$ -helix to  $\beta$ -hairpin transition in oligomeric aggregates of A $\beta$  has been characterized<sup>45</sup> by means of MD simulations.

When little experimental information about potential starting structures for the theoretical treatment is available or when the ergodicity is broken in the simulations, concepts beyond classical MD have to be employed. Among simulations that exploit pre-defined collective coordinates to push the sampling towards (or away from) desired regions of phase space, umbrella sampling<sup>46-48</sup>, steered molecular dynamics<sup>49,50</sup>, adaptive biasing force calculations<sup>51,52</sup>, metadynamics<sup>53,54</sup> and adaptively biased MD<sup>55,56</sup> are the most prominent ones. Complementary, replica exchange methods<sup>57-60</sup> can overcome free-energy barriers in a non-directed manner and can be often combined with the biasing techniques providing powerful exploration tools<sup>56,61</sup>. For A $\beta$  aggregation simulations, Tarus et al. used a protocol based on shape complementarity to generate an assortment of possible dimer structures and calculated the potentials of mean forces for dimerization<sup>62</sup>. Lately, Replica-exchange MD (REMD) has not only been used to study the aggregation process of several small amyloid peptides<sup>63</sup> and, more recently, the full length A $\beta$  1-40 dimer<sup>64</sup>, but also to investigate cross-seeding of Amyloid-protofibrils triggering tau-protein fibril formation<sup>65</sup>. A combination of a hybrid-resolution model with umbrella sampling and REMD was used by Schulzen et al. to obtain mechanistic and kinetic data for A $\beta$  fibril growth<sup>66</sup>.

Compared to the condensed phase examples given before, the gas-phase poses specific challenges to the structural exploration in theory: adding to the intrinsic flexibility of biomolecules, multiple charges and the absence of stabilizing interactions can alter the structure known from solution. At the same time, detailed structural representations like those derived by X-ray crystallography or NMR are not available for the gas-phase. Thus, combinations of systematic, enhanced sampling techniques or complementary experiments-driven structural explorations are most promising to find representative structures<sup>56,67-71</sup>.

The 12-28 fragment of the A $\beta$  protein (A $\beta$ <sub>12-28</sub>, VHHQKLVFAEDVGSNK) exhibits essentially identical neurotoxic behaviour and fibril formation as the full A $\beta$  protein<sup>72</sup> and is therefore a good model for gas-phase investigations. We recently tackled structural exploration of (monomeric) A $\beta$ <sub>12-28</sub> peptides in the gas-phase as a function of the charge state. We disclosed a strategy to sample structures of chromophore-grafted A $\beta$  peptides using replica-exchange MD and to reliably predict the FRET-efficiencies throughout the sample<sup>73</sup>. A follow-up study described the structural differences of Wildtype versus the F19P A $\beta$  alloform of the gas-phase systems<sup>74</sup>. In this contribution, we wish to extend the approach to aggregation and molecular recognition in order to

study the structure of A $\beta$  aggregates. We chose dimers of chromophore grafted A $\beta$ <sub>12-28</sub> - motivated by the fact that

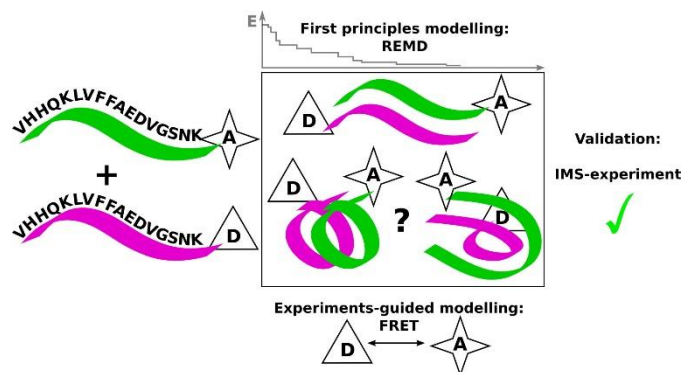


Figure 1: Concept of the theoretical and experimental structural exploration of chromophore grafted Amyloid- $\beta$  dimers in the gas-phase: Diversity of structures upon aggregation of two A $\beta$  stands is probed by two methodologies. First principles modelling using a REMD-based optimization strategy reveals low-energy conformations, FRET experiments-guided sampling (FRET between donor chromophore D and acceptor chromophore A) uses available experimental values for narrowing the searched phase space. The found structures are validated by complementary experiments from ion-mobility spectrometry.

dimers are the most abundant form of soluble A $\beta$  oligomers that can be detected in the human brain<sup>75</sup> and various neuropathological effects can be specifically attributed to their presence<sup>76</sup>.

We first introduce the A $\beta$  model composition employed throughout the theoretical treatment and the experiments. The structural exploration strategy is sketched in Figure 1: Global optimization of the dimer structure is performed from first principles using REMD. We then disclose a complementary experiments-guided method to sample structures with the aid of FRET measurements. We validate the choice of structural assignment by complementary experimental data – ion mobility cross sections. We discuss the findings in a broader context comparing the structures with available data from the condensed phase and rationalize them by an analysis of the sampled configurational space.

## Results

### A $\beta$ species in experiment and theory

In order to obtain conclusive FRET information about a dimer of the peptide, a donor and an acceptor chromophore must be grafted to each one of the units. We perform our simulation, action-FRET measurement and IMS experiments for C-terminally grafted A $\beta$ <sub>12-28</sub> dimers [(Ac-VHHQKLVFAEDVGSNKC<sup>Chr</sup>-NH<sub>2</sub>)<sub>2</sub>H]<sup>3+</sup> where C<sup>Chr</sup>-NH<sub>2</sub> denotes an NH<sub>2</sub> capped chromophore-C5 maleimide grafted cysteine residue, in analogy to previous experiments and calculations in our group<sup>73,74</sup>. We restrict our investigation further to a single charge state +3 because of its high intensity in the mass spectrum.

### Gas-phase optimization

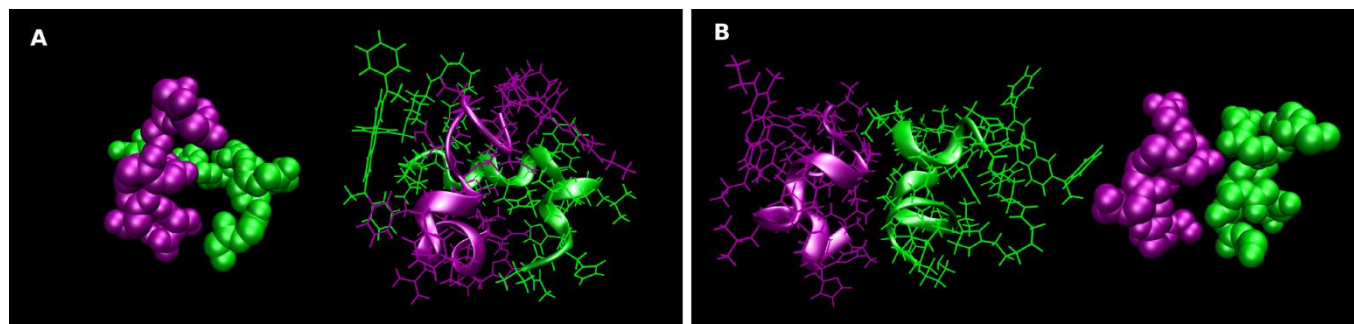


Figure 3: Visualization of the structural prototypes obtained A) by global optimization by REMD (strongly interacting) B) by FRET-experiments guided sampling (weakly interacting). The two peptide strands are colour coded with green and purple. A simplified peptide backbone representation is given to the left and to the right of the full structures.

In order to find the energetically most plausible dimer structure, we have performed a global optimization using replica exchange MD (REMD) that we have already used successfully for A $\beta$  monomers. A possible unbiased way to search for dimer structures is to compose it from the global minima of the monomers. As our modelling approach in Ref<sup>73</sup> turned out to be effective for doubly chromophore-grafted A $\beta$ <sub>12-28</sub>, we use the parametrization and sampling scheme reported therein (for details of the REMD calculations see “Computational details”). Because of the difference of charge state and labelling setup from previous work we started the global optimization of monomers from extended peptide conformations (see supplementary information, Figure S11). Based on pK<sub>a</sub> considerations for a total charge state of +3, we started REMD exploration of six monomer configurations (+1 charge state: all lysine residues neutral, LYN in Amber notation; +2 with protonated lysine, LYS, at positions K 16 or K 28. We selected the Rh575 grafted strand to feature the additional proton upon the lowest potential energy in isolated monomers. We cannot exclude in course of the dimer optimization this energetics might change and other protonation patterns are present – with presumably only little effect on the rather qualitative results reported herein

We have composed the dimer system by placing two A $\beta$ <sub>12-28</sub> monomer units separated by 15 nm and propagated a sequence of MD trajectories harmonically restraining the separation of chromophores R gradually from 15 to 2 nm similar to stratified umbrella sampling. The structures obtained at the end of umbrella sampling were used as starting structures for the follow-up optimization. So-composed starting structures for REMD have relatively high potential energies only little below the dissociation threshold of the configuration. In order to prevent dissociation in the initial REMD sampling cycles, we have set a chromophore-distance restraint amounting to 1.9 nm for 4 equilibration and REMD cycles (40 ns in each temperature) and removed the restraint, once a more favourable conformation was adopted. We continued non-restrained REMD until the potential energy of the lowest-energy optimized structure converged (4 further equilibration and REMD cycles, 20 ns in each temperature).

The final structure of this procedure is visualized in figure 2A. In the obtained structure, the peptide chains assume mostly helical secondary structure and are interlocked. Thus, it will be

termed the strongly interacting structure in the following. That

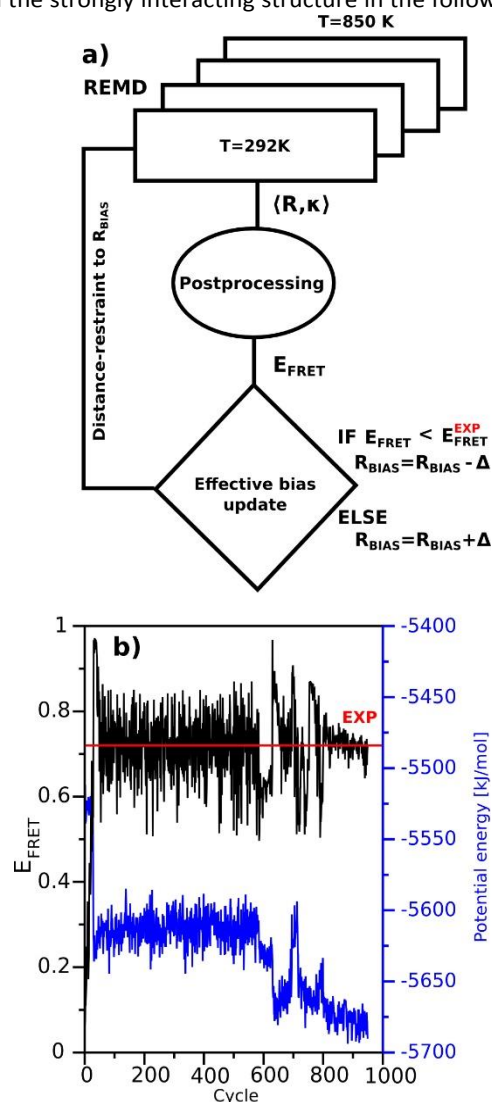


Figure 2: a) Workflow of the FRET-experiments guided sampling technique b) comparison of the average FRET efficiency of the ad-hoc sample (black line) for each biased REMD cycle in comparison with the experimental target value (red horizontal line) and potential energy of each sample's lowest-energy optimized structure (blue line).

such type of structure is preferred in the gas-phase seems plausible since the interlocking minimizes the surface of the dimer and maximizes its inter-strand interaction at the same time.

### FRET experiments-guided sampling

Opposed to the non-biased optimization we follow a complementary strategy, where we directly include the numerical value from the experimental gas-phase FRET measurement into the structural sampling. We have designed an adaptive biasing scheme that is based on replica-exchange MD and the prediction of ensemble-averaged FRET-efficiencies as described in Ref<sup>73</sup>. The proposed workflow of the adaptive method is detailed in Figure 2.

The idea of the approach is to check during the ongoing sampling, whether or not the current structural sample is compatible with the experimental average FRET efficiency and to adjust a restraint towards a region more compatible with experiments. The implementation follows the scheme in figure 3a: given a starting value for the bias position  $R_{\text{BIAS}}$  acting on the separation of the chromophores  $R$ , restrained replica-exchange MD simulations are propagated after a short equilibration period (see also “Computational Details”). The average FRET-efficiency  $E_{\text{FRET}}$  is predicted based on an ensemble of 100 structures with the distance  $R$  and orientational factor  $\kappa$  distribution taken from the 0.1 ns ambient-temperature trajectory. This prediction is compared with the experimental reference value. The target distance of the restraint  $R_{\text{BIAS}}$  is increased if the average FRET efficiency is smaller than found in the experiment or decreased otherwise. Two different step-sizes  $\Delta$  are chosen: when FRET-efficiencies differ by more than 0.1, a  $\Delta$  of  $\pm 0.1$  nm in the chromophore-separation restraint is attempted, while  $\Delta$  is set to 0.01 nm near the experimental value (average FRET efficiency within 0.1).

The replica-exchange sampling is able to overcome free energy barriers and is expected to converge towards the lowest free-energy sample at the given temperature that fulfils compatibility with the experimental FRET-efficiencies. The overall procedure could be regarded as establishing a weak and flexible cross-link between the two strands that imposes a guiding frame for the accessible conformational space. Notice that even covalent crosslinking of tyrosine residues in a recent experiment by Sitkiewicz et al.<sup>77</sup> only shifted the populations of  $A\beta$  dimers probed by IMS towards more compact forms but did not change the overall set of drift times. We therefore expect that during our simulations, the relatively soft restraint still allows for reasonable conformational dynamics, especially at the high temperatures of the REMD.

The progress and convergence of the procedure can be monitored as given in Figure 3b) by the calculated average FRET efficiency and the lowest potential energy in the sampling. After initial oscillations (quasi-free rotation of the two fragments) conformational jumps are made accessible upon the exchanges during REMD (about cycle 600, 60 ns, notice the significant drop of potential energy. Additional

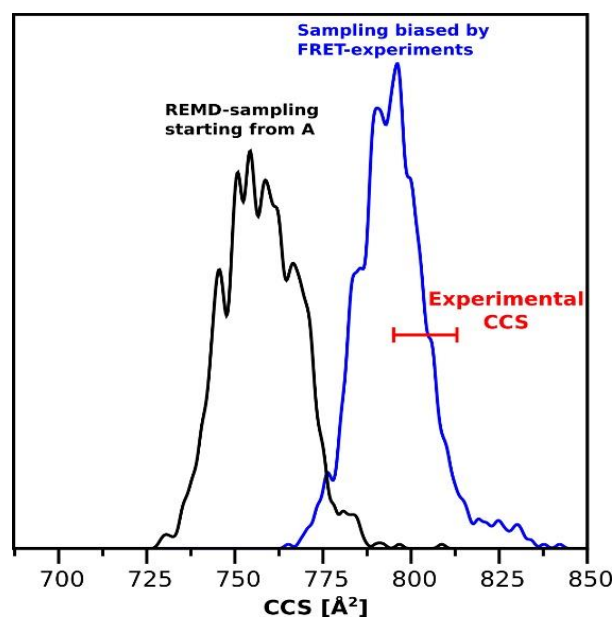


Figure 4: Validation of the modelled dimer structure families by IMS cross sections. Curves show the normalized probability density of a CCS value in the 292 K. Black: sample around found global minimum structure A. Blue: sample obtained after FRET-guided sampling. In red, the experimental average IMS cross section of the dimer is indicated.

moves (compatible with the experimental FRET) are found within the next 200 cycles after which the configuration only displays very minor structural changes.

The obtained (optimized) final structure from the biased sampling is visualized in figure 2B. Here, no interlocking (as found for structure A, figure 2A) is present. On the contrary, two globular units of  $A\beta_{12-28}$  interact in a stacked manner. In this way, intra-molecular interaction within each separate fragment is maximized. To increase the certainty with regard to their energetic characterization, we have re-optimized the structures A and B with the semi-empirical electronic structure method PM7<sup>78</sup>. These calculations confirmed that A is indeed lower in energy than B (by about 70 kJ/mol).

In conclusion, we have obtained two different structural families from a global optimization strategy and an experiments-guided strategy which makes a validation with the available experimental data necessary.

### Experimental validation of the structural types

In order to judge which of the structural families is present under the experimental conditions, we assess their compatibility with the available experimental data. It is obvious that B is compatible with the experimental FRET measurement since we used this information to guide the sampling. However, we still can judge the compatibility of A which has not been biased by the experimental information. The numerical value for the sample around A is 0.95 – significantly different from the experimental value (around 0.72) and therefore less compatible than B. This difference

might indicate that the global minimum of the dimer is not populated under the experimental conditions.

In order to assess this hypothesis, we exploit a second experiment that delivers structural information complementary to FRET. By comparing ion mobility cross-section measurements with theoretical predictions, we obtain shape information in addition to site-to-site distance from FRET. We calculated collisional cross sections (CCS) using the exact hard-spheres scattering model proposed by Shvartsburg et al.<sup>79</sup> upon the atomic coordinates of the samples around A and B. We display the theoretical and experimental CCS data in Figure 4 (the convergence of the CCS prediction upon the REMD samples for structure A is given in the supplementary information, Figure S12). The theoretical average CCS value amounts to 757 Å<sup>2</sup> for A and 795 Å<sup>2</sup> for B. The experimental CCS is determined to be around 804 Å<sup>2</sup>. Clearly, the structural family B is compatible with the experimental CCS value while A is not. From the fact that A is not compatible with both the FRET and CCS data, we conclude that the energetic global minimum – with maximized inter-peptide interaction is not present under the experimental conditions, but a relatively weakly bound aggregate of two compact chromophore grafted Aβ units.

## Discussion

The weakly interacting structure B may be formed during the electrospray process. It may also represent a kinetically trapped solution structure<sup>80</sup>.

The possibility to retain a non-global minimum configuration in the gas-phase requires the presence of a barrier dissecting the structure from other conformational families. As we have the REMD trajectories at higher temperatures available, we possess a large set of dimer configurations that we subject to a projection onto the transformation vector between A and B to identify the hypothesized barrier. From the 15 highest-temperature replica, 15,000 configurations were optimized to the next local minimum. We assume a hypothetical geometrical transformation from A → B (the strongly interacting structure towards the weakly interacting one). Because we are mainly interested in the biomolecular conformation, we use the backbone C, N and O atoms only (compare the backbone representation in figure 2). We project each configuration relative to B onto this transformation vector giving  $\xi$  as a measure for similarity either to A or to B. In figure 5, pairs of potential energies versus  $\xi$  are given. Any configuration on a connecting path between A and B assumes  $0 < \xi < 1$ . Thus, the characterization of all potential energies for configurations with  $0 < \xi < 1$  gives the *lower bound* for a barrier between A and B. Notice that we do not perform an analysis of the path itself and do not attempt to quantify this barrier. The lower bound of the barrier can be deduced from the minimum potential energies along  $\xi$  visualized by a blue line connecting potential energies of 49 bins of  $\xi$  between 0 and 1. Apparently, there exists a significant barrier to break self-interaction and partial unfolding to reorganize and build inter-strand interaction. This barrier renders it plausible that a weakly

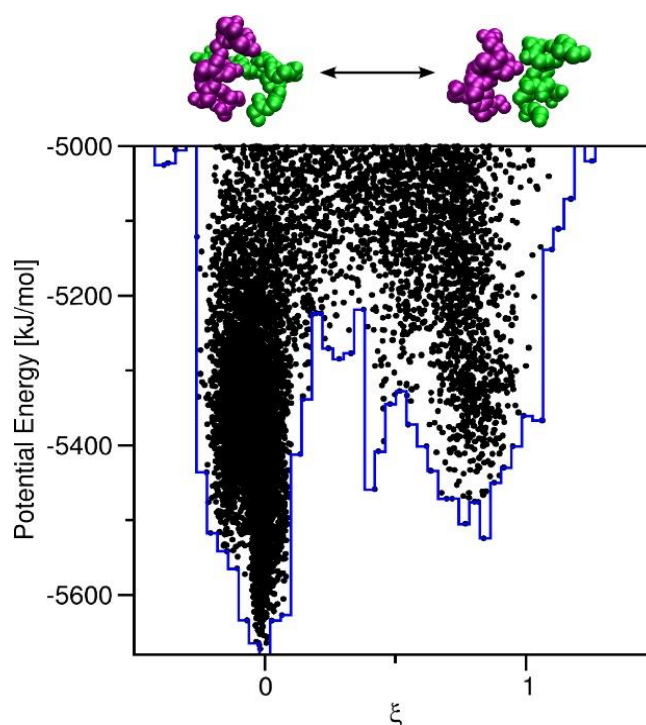


Figure 5: Potential energy of optimized configurations from high-temperature REMD sampling (starting structure A) versus its projection onto the vector connecting the structures A and B (black dots, transformation depicted above graph). Only peptide backbone atoms are used. Configurations with potential energies below -5,000 kJ/mol are shown only.  $\xi=0$  corresponds to overlap of the sampled configurations' backbone with the one of structure A, while  $\xi=1$  to overlap with B. The blue line connects lowest energies in the binned data indicating the lower bound for a barrier between A and B.

interacting structure B in the gas-phase is retained for long timescales.

In a recent theoretical endeavour using replica exchange MD, the equilibrium ensemble of Aβ<sub>1-40</sub> dimers was calculated<sup>64</sup>. The authors report a highly structurally disordered system with a large number of structures differing in secondary structure composition. The structure with third-highest population (S3) is strikingly similar to the weakly interacting configuration found in this work: two units with high helical content are in a stacked arrangement. It is therefore plausible that such solution structures are kinetically trapped and probed in gas-phase experiments.

In order to validate this viewpoint, we equilibrated the global gas-phase minimum (A) and the weakly interacting dimer (FRET-guided modelling, B) in explicit TIP3P water. The ambient-temperature trajectories (details and RMSD convergence of the simulation see supplementary information, Figure S13) show a retention of the interlocked (A) and stacked arrangement (B, in particular no dissociation) within 10 ns. To qualitatively judge the energetics for A and B in solution, we evaluated their PM7 energetics with implicit solvation (details see also Figure S13). While in the gas-phase, the strongly interacting structure (A) is significantly lower in energy than the weakly interacting structure (B), no such preference is present in solution (A and B are iso-energetic). Considering

that Tarus et al. do not evidence a major population of  $A\beta_{1-40}$  dimer resembling structure A, we suggest that A is not preferentially populated in solution and that barriers prevent transformation from B to A in the gas-phase.

## Conclusions

We have performed extensive theoretical structural exploration for chromophore-grafted  $A\beta_{12-28}$  peptide dimers in the gas-phase interfaced with structure-sensitive experiments: FRET and IMS. Gas-phase optimization of the dimer's conformation exploiting replica-exchange MD revealed an interlocked species as lowest in energy. We devised a complementary FRET-experiment-driven sampling procedure which - starting from the monomers' global minima - favoured a weakly interacting stacked arrangement. While the predicted FRET-efficiencies and ion-mobility cross-sections for the former are not consistent with the corresponding experimental data, the FRET and IMS cross-section predictions for the latter comply with both measurements. Although we cannot exclude that in our experiments the dimers form from isolated monomers during the electrospray process, the striking similarity of the weakly interacting configuration with one of the most probable  $A\beta_{1-40}$  dimer structures in solution at pH 7 suggests the possibility of a kinetically trapped solution structure. The presence of a high conformational barrier between the strongly and the weakly interacting species was evidenced by a projection of configurations generated in high-temperature trajectories of the REMD sampling. This analysis suggests that all paths from weakly to strongly interacting species have to pass through a maximum in potential energy, which in turn further strengthens the hypothesis of a solution-reminiscent kinetically trapped form of the chromophore-grafted  $A\beta_{12-28}$  peptide dimer. We linked gas-phase and solution simulations by equilibration in explicit solvent, suggesting that both prototype configurations are stable on a ns timescale. However, the energetic preference for the strongly interacting structure is not present in solution, rendering it possible that mostly weakly interacting dimers are probed, but free energy barriers prevent relaxation to the global minimum in the gas-phase. Our findings may have considerable impact for the ongoing research in the field of  $A\beta$  aggregation. Recent evidence from ion mobility indicates that the aggregation characteristics and mechanisms need further investigations because SDS-PAGE analysis technique might be biased through the formation of crosslinks<sup>25,26</sup>. Likewise, cryo-EM generated structural models of  $A\beta_{1-42}$  differ from earlier models with U-shaped structure<sup>81,82</sup> but highlight the importance of dimers and postulate that for  $A\beta_{1-42}$ , intermediates or nuclei consist of 2n monomers. These latest developments underline the necessity for complementary structure-determining approaches, e.g. by gas-phase experiments combined with atomistic modelling and guided sampling as presented in this paper - that will help to establish a unified view of  $A\beta$  oligomerization and its importance for Alzheimer's disease.

## Computational details

Classical molecular dynamics (MD) simulations were performed based on the AMBER99 force field<sup>83,84</sup> that was completed with the generalized Amber Force Field (GAFF) to describe the non-standard chromophore grafted cysteine residues.<sup>33-35</sup> For the MD simulations, Gromacs 5.0.2 was used using the Velocity-Verlet integration algorithm with a time-step of 1 fs in absence of any cut-offs for the evaluation of interactions.<sup>36-38</sup> Preparative stratified umbrella-sampling calculations were performed with harmonically restraining ( $100 \text{ kJmol}^{-1}\text{nm}^{-1}$ ) the chromophore separation represented by the xanthene-O-O distance. Global optimization of monomers and dimers employed a sequence of replica-exchange molecular dynamics simulations (REMD). REMD was done with 20 trajectories in parallel which were assigned to temperatures from 220 to 850 K in frame of the velocity-rescaling algorithm that includes a stochastic term for the correct representation of a Boltzmann ensemble.<sup>39</sup> Exchange attempts between adjacent replicas were performed every 200 steps leading to exchange probabilities of about 20 % for the monomers in average. After local optimization and a short 100 ps equilibration at each temperature, a 10 ns REMD was started and every 1,000<sup>th</sup> structure of the 220 K and 292 K ensembles were taken as samples. The lowest-energy optimized structure of the 220 K ensemble was taken as a new starting point and the procedure was repeated until the potential energy distribution and the energy of the optimized lowest-energy structure had converged. Preparatory restrained REMD of the gas-phase optimization used a Ratchet-and-Pawl like scheme<sup>85,86</sup> as implemented in PLUMED<sup>87</sup> that can be used to evolve collective variables towards a target value (here 1.9 nm) using a harmonic potential (force constant  $100 \text{ kJmol}^{-1}\text{nm}^{-1}$ ) propelled by the thermal fluctuations and without work on the system. The average exchange probabilities lie around 10%. After 4 of such cycles (40 ns), we refined the REMD sampling with extending the used temperatures to 32 values between 200 and 900 K. The restraint was replaced with an upper wall to the chromophore separation placed at 7 nm that prevented numerical instabilities from exchanges to very distant monomers (we also chose a smaller time step of 0.5 fs to increase the numerical stability for exchanges to high-temperature replica). The procedure yielded exchange probabilities of 22-30 % in average with 1.2 effective exchanges per ps for each replica. The diffusive behaviour of the nuclear trajectory with ambient starting temperature within the relevant temperature space is given in the supplementary information, Figure SI4.

In the adaptive FRET-experiments-guided sampling, an equilibration for 1 ps at every temperature was performed in each cycle before the production. Restrained REMD (restraining done as described before but using an updated target value in each cycle) is then propagated for 0.1 ns with a 1 fs time step and with attempted exchanges every 100 steps. The chosen trajectory length provided enough exchange attempts (1000) so that conformational jumps can be

achieved. The calculation of FRET-efficiency exploited Förster Theory as detailed in references<sup>40,41</sup>. The distance distribution between the optically active units of the chromophores is calculated by evaluation of the geometrical centre of all atoms in the xanthene moiety and the N-linked side chains. The FRET-efficiency distribution is then calculated from the chromophore distance and chromophore-orientation distributions. The ensemble-averaged value is then compared with the experimental data. The CCS for the comparison with ion-mobility data were obtained by invoking the exact hard-spheres scattering method originally proposed by Shvartsburg *et al.* implemented locally.<sup>42</sup>

## Experiments

Carboxyrhodamine 575 C<sub>5</sub>-maleimide (Setareh Biotech) (R575) and QSY 7 C<sub>5</sub>-maleimide (Life Technologies) (QSY7) were used as donor and acceptor chromophores for action-FRET measurements respectively. A $\beta$ <sub>12-28</sub> with C-terminal cysteine residue (Ace-V<sup>12</sup>HHQKLVFFAEDVGSNK<sup>28</sup>C-NH<sub>2</sub>) were purchased from Genecust (Luxembourg) and each dissolved in a 1:1 mixture of H<sub>2</sub>O:acetonitrile to a concentration of ~500  $\mu$ M. Chromophores were grafted by adding equimolar quantities to the aforementioned stock solution. 100  $\mu$ l of each reaction solution was added to 2 ml H<sub>2</sub>O:acetonitrile for use in the electrospray source.

A linear quadrupole ion trap mass spectrometer was used to generate, mass select and trap ions in a first, high pressure ion trap for a controlled duration. A fused silica window is positioned at the back end of the instrument and allows for the introduction of the lasers in the UV-visible range along the ion traps axis. Fragment ions are transmitted to a second ion trap, with a low pressure, where they are analysed. The light source used is a Panther EX OPO pumped by the third harmonic (355 nm) of a Surelite II Nd:YAG laser (Continuum, Santa Clara, CA). A repetition rate of 10 Hz and pulse-widths of the order of 5 ns were used. Pulse energies were kept between 1.0 to 4.5 mJ/pulse to avoid saturation. A mechanical shutter, synchronized with the mass spectrometer, is used to stop the beam at all times except the 'ion activation window' – that is the time after ion accumulation and before the mass analysis. A single laser pulse was used for the irradiation of the trapped ions. When irradiating ions the normalized collision energy is kept at zero.

For action-FRET, measurements were taken at wavelengths of 505 nm and 545 nm, corresponding to the absorption maxima of the donor and acceptor chromophores respectively. Action-FRET efficiencies are calculated as the ratio of acceptor specific fragmentation at 505 nm to that at 545 nm, normalized to the photon flux, as described previously<sup>28</sup>. To account for the influence of direct absorption and fragmentation of the acceptor at 505 nm a correction of – 0.25 (corresponding to the ratio of the fragmentation efficiency of the acceptor chromophore at 505 and 545 nm) was applied to all FRET efficiencies.

Ion mobility (IMS) measurements were performed using a custom-built tandem ion mobility spectrometer already

described elsewhere<sup>88</sup>. Briefly, two drift tubes, each 79 cm long, are inserted between an electrospray ionization source and a time-of-flight (ToF) mass spectrometer. Herein, we used only the second drift tube to measure CCS of the A $\beta$  dimer. Helium at a pressure of 3.45 Torr is maintained in the drift tube, and the temperature of the whole setup is kept at 300 K. Their mass-to-charge ratio and drift time through the tube are simultaneously measured using the ToF. CCS is finally calculated from the evolution of the ion arrival time distribution as a function of the inverse drift voltage<sup>89</sup>.

## Acknowledgements

Computer time granted by the P2HPD (Pôle de Calcul Hautes Performances Dédiés, Université Lyon 1) is gratefully acknowledged. A.K. acknowledges funding from the Deutsche Forschungsgemeinschaft DFG (Research Fellowship Ku 3251/1-1) and support by COST Actions BM1403 and CM1405. The research leading to these results has received funding from the European Research Council under the European Union's Seventh Framework Programme (FP7/2007-2013 Grant agreement No. 320659).

## References

- 1 C. Haass and D. J. Selkoe, *Nat. Rev. Mol. Cell Biol.*, 2007, **8**, 101–112.
- 2 J. Hardy and D. J. Selkoe, *Science*, 2002, **297**, 353–356.
- 3 R. Roychoudhuri, M. Yang, M. M. Hoshi and D. B. Teplow, *J. Biol. Chem.*, 2009, **284**, 4749–4753.
- 4 A. K. Paravastu, I. Qahwash, R. D. Leapman, S. C. Meredith and R. Tycko, *Proc. Natl. Acad. Sci. U. S. A.*, 2009, **106**, 7443–7448.
- 5 K. Ono, M. M. Condrón and D. B. Teplow, *Proc. Natl. Acad. Sci. U. S. A.*, 2009, **106**, 14745–50.
- 6 M. Ahmed, J. Davis, D. Aucoin, T. Sato, S. Ahuja, S. Aimoto, J. I. Elliott, W. E. Van Nostrand and S. O. Smith, *Nat. Struct. Mol. Biol.*, 2010, **17**, 561–567.
- 7 L. Yu, R. Edalji, J. E. Harlan, T. F. Holzman, A. P. Lopez, B. Labkovsky, H. Hillen, S. Barghorn, U. Ebert, P. L. Richardson, L. Miesbauer, L. Solomon, D. Bartley, K. Walter, R. W. Johnson, P. J. Hajduk and E. T. Olejniczak, *Biochemistry*, 2009, **48**, 1870–1877.
- 8 S. L. Bernstein, N. F. Dupuis, N. D. Lazo, T. Wyttenbach, M. M. Condrón, G. Bitan, D. B. Teplow, J.-E. Shea, B. T. Ruotolo, C. V. Robinson and M. T. Bowers, *Nat. Chem.*, 2009, **1**, 326–331.
- 9 T. Härd and C. Lendel, *J. Mol. Biol.*, 2012, **421**, 441–465.
- 10 G. von Helden, P. R. Kemper, N. G. Gotts and M. T. Bowers, *Science (80-. )*, 1993, **259**, 1300–1302.
- 11 D. E. Clemmer and M. F. Jarrold, *J. Mass Spectrom.*, 1997, **32**, 577–592.

- 12 J. A. Silveira, K. L. Fort, D. Kim, K. A. Servage, N. A. Pierson, D. E. Clemmer and D. H. Russell, *J. Am. Chem. Soc.*, 2013, **135**, 19147–53.
- 13 S. L. Koeniger, S. I. Merenbloom, S. J. Valentine, M. F. Jarrold, H. R. Udseth, R. D. Smith, D. E. Clemmer, W. A. Hill, E. Molecular, P. Northwest and P. O. Box, *Anal. Chem.*, 2006, **78**, 4161–4174.
- 14 M. F. Bush, I. D. G. Campuzano and C. V Robinson, *Anal. Chem.*, 2012, **84**, 7124–30.
- 15 D. E. Clemmer and M. F. Jarrold, *J. Mass Spectrom.*, 1997, **32**, 577–592.
- 16 A. A. Shvartsburg, R. R. Hudgins, P. Dugourd and M. F. Jarrold, *Chem. Soc. Rev.*, 2001, **30**, 26–35.
- 17 P. Dugourd, R. R. Hudgins, D. E. Clemmer and M. F. Jarrold, *Rev. Sci. Instrum.*, 1997, **68**, 1122–1129.
- 18 T. Wyttenbach and M. T. Bowers, *Mod. Mass Spectrom.*, 2003, **225**, 207–232.
- 19 C. Uetrecht, R. J. Rose, E. van Duijn, K. Lorenzen and A. J. R. Heck, *Chem. Soc. Rev.*, 2010, **39**, 1633–55.
- 20 C. Bleiholder, N. F. Dupuis, T. Wyttenbach and M. T. Bowers, *Nat. Chem.*, 2011, **3**, 172–177.
- 21 T. W. Knapman, N. M. Valette, S. L. Warriner and a E. Ashcroft, *Curr. Anal. Chem.*, 2013, **9**, 181–191.
- 22 F. Canon, R. Ballivian, F. Chiro, R. Antoine, P. Sarni-Manchado, J. Lemoine and P. Dugourd, *J. Am. Chem. Soc.*, 2011, **133**, 7847–7852.
- 23 L. M. Young, P. Cao, D. P. Raleigh, A. E. Ashcroft and S. E. Radford, *J. Am. Chem. Soc.*, 2014, **136**, 660–70.
- 24 S.-H. Chen and D. H. Russell, *J. Am. Soc. Mass Spectrom.*, 2015, **26**, 1433–43.
- 25 R. Pujol-Pina, S. Vilapinyó-Pascual, R. Mazzucato, A. Arcella, M. Vilaseca, M. Orozco and N. Carulla, *Sci. Rep.*, 2015, **5**, 14809.
- 26 A. D. Watt, K. a. Perez, A. Rembach, N. a. Sherrat, L. W. Hung, T. Johanssen, C. a. McLean, W. M. Kok, C. a. Hutton, M. Fodero-Tavoletti, C. L. Masters, V. L. Villemagne and K. J. Barnham, *Acta Neuropathol.*, 2013, **125**, 549–564.
- 27 D. Thirumalai, G. Reddy and J. E. Straub, *Acc. Chem. Res.*, 2012, **45**, 83–92.
- 28 T. Forster, *Naturwissenschaften*, 1946, **33**, 166–175.
- 29 G. D. Scholes, *Annu. Rev. Phys. Chem.*, 2003, **54**, 57–87.
- 30 P. R. Selvin, *Nat. Struct. Biol.*, 2000, **7**, 730–734.
- 31 V. Frankevich, V. Chagovets, F. Widjaja, K. Barylyuk, Z. Y. Yang and R. Zenobi, *Phys. Chem. Chem. Phys.*, 2014, **16**, 8911–8920.
- 32 S. Daly, F. Poussiguet, A.-L. Simon, L. MacAleese, F. Bertorelle, F. Chiro, R. Antoine and P. Dugourd, *Anal. Chem.*, 2014.
- 33 V. Frankevich, V. Chagovets, F. Widjaja, K. Barylyuk, Z. Yang and R. Zenobi, *Phys. Chem. Chem. Phys.*, 2014, **16**, 8911–20.
- 34 F. O. Talbot, A. Rullo, H. Yao and R. a. Jockusch, *J. Am. Chem. Soc.*, 2010, **132**, 16156–16164.
- 35 R. Zenobi, *Anal. Chem.*, 2015, **87**, 7497–7498.
- 36 B. Schuler, E. A. Lipman, P. J. Steinbach, M. Kumke and W. A. Eaton, *Proc. Natl. Acad. Sci. U. S. A.*, 2005, **102**, 2754–9.
- 37 L. Stryer, *Annu. Rev. Biochem.*, 1978, **47**, 819–46.
- 38 S. B. Nabuurs, C. A. E. M. Spronk, E. Krieger, H. Maassen, G. Vriend and G. W. Vuister, *J. Am. Chem. Soc.*, 2003, **125**, 12026–12034.
- 39 P. Robustelli, K. Kohlhoff, A. Cavalli and M. Vendruscolo, *Structure*, 2010, **18**, 923–933.
- 40 M. Magnus, D. Matelska, G. Lach, G. Chojnowski, M. J. Boniecki, E. Purta, W. Dawson, S. Dunin-Horkawicz and J. M. Bujnicki, *RNA Biol.*, 2014, **11**, 1–15.
- 41 S. Kalinin, T. Peulen, S. Sindbert, P. J. Rothwell, S. Berger, T. Restle, R. S. Goody, H. Gohlke and C. a M. Seidel, *Nat. Methods*, 2012, **9**, 1218–1227.
- 42 J. Khandogin and C. L. Brooks, *Proc. Natl. Acad. Sci. U. S. A.*, 2007, **104**, 16880–16885.
- 43 U. F. Röhrig, A. Laio, N. Tantalò, M. Parrinello and R. Petronzio, *Biophys. J.*, 2006, **91**, 3217–3229.
- 44 X. Zhu, R. P. Bora, A. Barman, R. Singh and R. Prabhakar, *J. Phys. Chem. B*, 2012, **116**, 4405–4416.
- 45 F. Simona, G. Tiana, R. A. Broglia and G. Colombo, *J. Mol. Graph. Model.*, 2004, **23**, 263–273.
- 46 G. M. Torrie and J. P. Valleau, *J. Comput. Phys.*, 1977, **23**, 187–199.
- 47 P. Virnau and M. Müller, *J. Chem. Phys.*, 2004, **120**, 10925–10930.
- 48 J. Kästner, *Wiley Interdiscip. Rev. Comput. Mol. Sci.*, 2011, **1**, 932–942.
- 49 S. Izrailev, S. Stepaniants, B. Isralewitz, D. Kosztin, H. Lu, F. Molnar, W. Wriggers and K. Schulten, in *Computational Molecular Dynamics: Challenges, Methods, Ideas SE - 2*, 1999, vol. 4, pp. 39–65.
- 50 S. Park and K. Schulten, *J. Chem. Phys.*, 2004, **120**, 5946–5961.
- 51 K. Minoukadeh, C. Chipot and T. Lelièvre, *J. Chem. Theory Comput.*, 2010, **6**, 1008–1017.
- 52 T. Lelievre, F. Otto, M. Rousset and G. Stoltz, *Nonlinearity*, 2007, **21**, 1155–1181.
- 53 B. Ensing, M. De Vivo, Z. Liu, P. Moore and M. L. Klein, *Acc. Chem. Res.*, 2006, **39**, 73–81.
- 54 A. Laio and M. Parrinello, *Proc. Natl. Acad. Sci. U. S. A.*, 2002, **99**, 12562–12566.
- 55 V. Babin, V. Karpusenka, M. Moradi, C. Roland and C. Sagui,

- in *International Journal of Quantum Chemistry*, 2009, vol. 109, pp. 3666–3678.
- 56 F. Calvo, F. Chiro, F. Albrieux, J. Lemoine, Y. O. Tsybin, P. Pernot and P. Dugourd, *J. Am. Soc. Mass Spectrom.*, 2012, **23**, 1279–1288.
- 57 J. Kim, T. Keyes and J. E. Straub, *J. Chem. Phys.*, 2010, **132**, 224107.
- 58 Y. M. Rhee and V. S. Pande, *Biophys. J.*, 2003, **84**, 775–786.
- 59 Y. Sugita, A. Kitao and Y. Okamoto, *J. Chem. Phys.*, 2000, **113**, 6042–6051.
- 60 Y. Sugita and Y. Okamoto, *Chem. Phys. Lett.*, 1999, 314, 141–151.
- 61 F. Chiro, F. Calvo, F. and Albrieux, J. Lemoine, Y. O. Tsybin and P. Dugourd, *J. Am. Soc. Mass Spectrom.*, 2012, **23**, 386–396.
- 62 B. Tarus, J. E. Straub and D. Thirumalai, *J. Mol. Biol.*, 2005, **345**, 1141–1156.
- 63 M. Cecchini, F. Rao, M. Seeber and A. Caflisch, *J. Chem. Phys.*, 2004, **121**, 10748.
- 64 B. Tarus, T. T. Tran, J. Nasica-Labouze, F. Sterpone, P. H. Nguyen and P. Derreumaux, *J. Phys. Chem. B*, 2015, **119**, 10478–87.
- 65 R. Qi, Y. Luo, G. Wei, R. Nussinov and B. Ma, *J. Phys. Chem. Lett.*, 2015, 150806105346002.
- 66 W. Han and K. Schulten, *J. Am. Chem. Soc.*, 2014, **136**, 12450–60.
- 67 P. Poulain, F. Calvo, R. Antoine, M. Broyer and P. Dugourd, *Phys. Rev. E*, 2006, **73**, 056704.
- 68 F. Calvo, F. Chiro, F. Albrieux, J. Lemoine, Y. O. Tsybin, P. Pernot and P. Dugourd, *J. Am. Soc. Mass Spectrom.*, 2012, **23**, 1279–1288.
- 69 F. Albrieux, F. Calvo, F. Chiro, A. Vorobyev, Y. O. Tsybin, V. Lepère, R. Antoine, J. Lemoine and P. Dugourd, *J. Phys. Chem. A*, 2010, **114**, 6888–6896.
- 70 F. Calvo and P. Dugourd, *J. Phys. Chem. A*, 2008, **112**, 4679–87.
- 71 F. Chiro, F. Calvo, F. Albrieux, J. Lemoine, Y. O. Tsybin and P. Dugourd, *J. Am. Soc. Mass Spectrom.*, 2012, **23**, 386–96.
- 72 P. E. Fraser, L. Lévesque and D. R. McLachlan, *J. Neurochem.*, 1994, **62**, 1227–1230.
- 73 A. Kulesza, S. Daly, L. MacAleese, R. Antoine and P. Dugourd, *J. Chem. Phys.*, 2015, **143**, 025101.
- 74 S. Daly, A. Kulesza, F. Poussigues, A.-L. Simon, C. M. Choi, G. Knight, F. Chiro, L. MacAleese, R. Antoine and P. Dugourd, *Chem. Sci.*, 2015, **6**, 5040–5047.
- 75 M. Jin, N. Shepardson, T. Yang, G. Chen, D. Walsh and D. J. Selkoe, *Proc. Natl. Acad. Sci. U. S. A.*, 2011, **108**, 5819–5824.
- 76 G. M. Shankar, S. Li, T. H. Mehta, A. Garcia-Munoz, N. E. Shepardson, I. Smith, F. M. Brett, M. A. Farrell, M. J. Rowan, C. A. Lemere, C. M. Regan, D. M. Walsh, B. L. Sabatini and D. J. Selkoe, *Nat. Med.*, 2008, **14**, 837–842.
- 77 E. Sitkiewicz, J. Ołędzki, J. Poznański and M. Dadlez, *PLoS One*, 2014, **9**, e100200.
- 78 J. J. P. Stewart, *J. Mol. Model.*, 2013, **19**, 1–32.
- 79 A. A. Shvartsburg and M. F. Jarrold, *Chem. Phys. Lett.*, 1996, 261, 86–91.
- 80 H. L. Shi, N. Atlasevich, S. I. Merenbloom and D. E. Clemmer, *J. Am. Soc. Mass Spectrom.*, 2014, **25**, 2000–2008.
- 81 T. Lührs, C. Ritter, M. Adrian, D. Riek-Loher, B. Bohrmann, H. Döbeli, D. Schubert and R. Riek, *Proc. Natl. Acad. Sci. U. S. A.*, 2005, **102**, 17342–17347.
- 82 R. Tycko, *Annu. Rev. Phys. Chem.*, 2011, **62**, 279–299.
- 83 D. A. Pearlman, D. A. Case, J. W. Caldwell, W. S. Ross, T. E. Cheatham, S. DeBolt, D. Ferguson, G. Seibel and P. Kollman, *Comput. Phys. Commun.*, 1995, 91, 1–41.
- 84 J. Wang, P. Cieplak and P. a Kollman, *J. Comput. Chem.*, 2000, **21**, 1049–1074.
- 85 M. Marchi and P. Ballone, *J. Chem. Phys.*, 1999, **110**, 3697.
- 86 D. Provasi and M. Filizola, *Biophys. J.*, 2010, **98**, 2347–2355.
- 87 M. Bonomi, D. Branduardi, G. Bussi, C. Camilloni, D. Provasi, P. Raiteri, D. Donadio, F. Marinelli, F. Pietrucci, R. A. Broglia and M. Parrinello, *Comput. Phys. Commun.*, 2009, **180**, 1961–1972.
- 88 A.-L. Simon, F. Chiro, C. M. Choi, C. Clavier, M. Barbaire, J. Maurelli, X. Dagany, L. MacAleese and P. Dugourd, *Rev. Sci. Instrum.*, 2015, **86**, 094101.
- 89 H. E. Revercomb and E. A. Mason, *Anal. Chem.*, 1975, **47**, 970–983.